Eur. Phys. J. B **52**, 133–142 (2006)
DOI: 10.1140/epjb/e2006-00276-8

THE EUROPEAN PHYSICAL JOURNAL B

Electronic structure and g factors of narrow-gap zinc-blende nanowires and nanorods

X.W. Zhang[a], Y.H. Zhu, and J.B. Xia

Chinese Center of Advanced Science and Technology (World Laboratory), P.O. Box 8730, Beijing 100080, P.R. China
and
Institute of Semiconductors, Chinese Academy of Sciences, P.O. Box 912, Beijing 100083, P.R. China

Received 9 May 2006
Published online 6 July 2006 –

Abstract. The Hamiltonian in the framework of eight-band effective-mass approximation of the zinc-blende nanowires and nanorods in the presence of external homogeneous magnetic field is given in the cylindrical coordinate. The electronic structure, optical properties, magnetic energy levels, and g factors of the nanowires and nanorods are calculated. It is found that the electron states consist of many hole-state components, due to the coupling of the conduction band and valence band. For the normal bands which are monotone functions of $|k_z|$, long nanorods can be modeled by the nanowires, the energy levels of the nanorods approximately equal the values of the energy band $E(k_z)$ of the nanowires with the same radius at a special k_z, where k_z is the wave vector in the wire direction. Due to the coupling of the states, some of the hole energy bands of the nanowires have their highest points at $k_z \neq 0$. Especially, the highest hole state of the InSb nanowires is not at the $k_z = 0$ point. It is an indirect band gap. For these abnormal bands, nanorods can not be modeled by the nanowires. The energy levels of the nanorods show an interesting plait-like pattern. The linear polarization factor is zero, when the aspect ratio $L/2R$ is smaller than 1, and increases as the length increases. The g_z and g_x factors as functions of the k_z, radius R and length L are calculated for the wires and rods, respectively. For the wires, the g_z of the electron ground state increases, and the g_z of the hole ground state decreases first, then increases with the k_z increasing. For the rods, the g_z and g_x of the electron ground state decrease as the R or the L increases. The g_x of the hole ground state decreases, the g_z of the hole ground state increases with the L increasing. The variation of the g_z of the wires with the k_z is in agreement with the variation of the g_z of the rods with the L.

PACS. 73.21.La Quantum dots – 73.21.Hb Quantum wires – 75.75.+a Magnetic properties of nanostructures – 78.67.Hc Quantum dots

1 Introduction

Narrow-gap semiconductors have been discussed for their special characteristics. It gives rise to a lot of interesting physical effects, as well as useful technological applications, such as infrared detectors and lasers.

For the wide use of applications, people pay more and more attention to the narrow-gap semiconductors. Regarded as the typical example, lots of investigations on InAs and InSb nanowires and nanorods have been reported in decades. InAs nanowires and whiskers were grown by reaction of indium with GaAs [1]. InAs nanorods were synthesized by colloidal chemistry techniques [2,3], whose length-dependent optical properties [2] and tunnelling spectra [3] were measured. InSb nanowires and nanorods are also synthesized [4–6]. Luttinger-liquid-like transport in long InSb nanowires were studied [6]. Energy spectrum [7,8], electron and hole g factors [9,10], linear polarized absorption and emission [11], spin-orbit coupling effects[12], and one-dimensional excitons [13–15] of these low-dimensional systems were investigated. Single nanowire lasers were made out [16].

Motivated by the experimental progress, we study the electronic structure, optical properties and g factors of narrow-gap zinc-blende nanowires and nanorods in the framework of the eight-band effective-mass approximation. It is found that the long nanorods can be modeled by the nanowires, and the energy levels of the nanorods equal the values of the energy band $E(k_z)$ of the nanowires with the same radius at a special k_z, where k_z is the wave vector in the wire direction. The remainder of this paper is organized as follows. In Section 2 we give the form of

[a] e-mail: zhxw99@semi.ac.cn

the Hamiltonian. Our numerical results and discussions are given in Section 3. Finally, we draw a brief conclusion in Section 4.

2 Theory model and calculations

In the absence of external magnetic field, we represent the eight-band effective-mass Hamiltonian in the Bloch function bases $|S\rangle\uparrow$, $|11\rangle\uparrow$, $|10\rangle\uparrow$, $|1-1\rangle\uparrow$, $|S\rangle\downarrow$, $|11\rangle\downarrow$, $|10\rangle\downarrow$, $|1-1\rangle\downarrow$ as

$$H_{eb} = \begin{pmatrix} H_{int} & \\ & H_{int} \end{pmatrix} + H_{so}. \tag{1}$$

H_{so} is the valence band spin-orbit coupling Hamiltonian [17].

H_{int} is written as

$$H_{int} = \frac{1}{2m_0}\begin{pmatrix} \epsilon_g + P_e & \frac{i}{\sqrt{2}}p_0 p_+ & ip_0 p_z & \frac{i}{\sqrt{2}}p_0 p_- \\ -\frac{i}{\sqrt{2}}p_0 p_- & -P_1 & -S & -T \\ -ip_0 p_z & -S^\star & -P_3 & -S \\ -\frac{i}{\sqrt{2}}p_0 p_+ & -T^\star & -S^\star & -P_1 \end{pmatrix} \tag{2}$$

where

$$P_e = \alpha p_- p_+ + \alpha p_z^2, \tag{3a}$$

$$P_1 = \frac{L'+M'}{2}p_- p_+ + M' p_z^2, \tag{3b}$$

$$P_3 = M' p_- p_+ + L' p_z^2, \tag{3c}$$

$$T = \frac{L'-M'-N'}{4}p_+^2 + \frac{L'-M'+N'}{4}p_-^2, \tag{3d}$$

$$T^* = \frac{L'-M'-N'}{4}p_-^2 + \frac{L'-M'+N'}{4}p_+^2, \tag{3e}$$

$$S = \frac{1}{\sqrt{2}}N' p_- p_z, \tag{3f}$$

$$S^* = \frac{1}{\sqrt{2}}N' p_+ p_z, \tag{3g}$$

$$p_\pm = p_x \pm i p_y. \tag{3h}$$

$\epsilon_g = 2m_0 E_g$, and E_g is the bandgap of bulk material. $p_0 = \sqrt{2m_0 E_P}$, and E_P is the matrix element of Kane's theory.

As we have take into account the coupling of valence band and conduction band, the Luttinger parameters L and N should subtract the contribution from conduction band [18], that is to say, $L' = L - E_p/E_g$, $N' = N - E_p/E_g$. M does not change, $M' = M$. The electron effective mass should also subtract the contribution from valence band [19],

$$\alpha = \frac{m_0}{m_c} - \frac{E_p}{3}\left[\frac{2}{E_g} + \frac{1}{E_g + \Delta_{so}}\right]. \tag{4}$$

where m_c is the electron effective mass and Δ_{so} is the spin-orbital splitting energy of the valence band.

We assume that the electrons and holes are confined in a infinitely high potential barrier. In the spherical-symmetry approximation, the transverse envelope function can be expanded with Bessel functions. The longitudinal envelope function of the nanowires is the plane wave $e^{ik_z z}$, where k_z is the continuum wave vector along the z direction, which is the wire direction. Approximately, the longitudinal envelope function of the nanorods is written as $e^{izm\pi/L}$, $m = 1, 2, 3, ...$, simply replacing the continuum wave vector k_z by $m\pi/L$ [20]. We call this approximate calculation of the nanorods the Wire Model. For more exact calculation, we assume that the longitudinal envelope function can be expanded with Sine functions,

$$|m\rangle = \sqrt{\frac{2}{L}}\sin(m\frac{\pi}{L}z), m = 1, 2, 3, ... \tag{5}$$

We call this calculation of the nanorods the Rod Model. We should say that it is very hard to do the calculation in the Rod Model for long nanorods, numerous basic functions should be included as the p_z linear terms in the Haniltonian [Eq. (2)] couple different $|m\rangle$ states as follows

$$\langle m'|p_z|m\rangle = \frac{\hbar}{i}\frac{1}{L}\frac{4m'm}{(m'-m)(m'+m)}, \tag{6}$$

if m' and m have different parities, else $= 0$. Actually, the Wire Model ignores this coupling.

The total envelope function including the electron and hole states is written as

$$\Psi_{J,k_z\ (\text{or } m)} = \begin{pmatrix} e_{l,n,\uparrow}A_{l,n}J_l\left(k_n^l r\right)e^{il\theta} \\ b_{l-1,n,\uparrow}A_{l-1,n}J_{l-1}\left(k_n^{l-1} r\right)e^{i(l-1)\theta} \\ c_{l,n,\uparrow}A_{l,n}J_l\left(k_n^l r\right)e^{il\theta} \\ d_{l+1,n,\uparrow}A_{l+1,n}J_{l+1}\left(k_n^{l+1} r\right)e^{i(l+1)\theta} \\ e_{l+1,n,\downarrow}A_{l+1,n}J_{l+1}\left(k_n^{l+1} r\right)e^{i(l+1)\theta} \\ b_{l,n,\downarrow}A_{l,n}J_L\left(k_n^l r\right)e^{il\theta} \\ c_{l+1,n,\downarrow}A_{l+1,n}J_{l+1}\left(k_n^{l+1} r\right)e^{i(l+1)\theta} \\ d_{l+2,n,\downarrow}A_{l+2,n}J_{l+2}\left(k_n^{l+2} r\right)e^{i(l+2)\theta} \end{pmatrix} \times e^{ik_z z}\ (\text{or } e^{i\pi m z/L} \text{or } |m\rangle), \tag{7}$$

where $J = l + 1/2$ is the total angular momentum, which is a good quantum number in the absence of transversely applied magnetic field. And $A_{l,n}$ is the normalization constant,

$$A_{l,n} = \frac{1}{\sqrt{\pi}RJ_{l+1}\left(\alpha_n^l\right)}. \tag{8}$$

$\alpha_n^l = k_n^l R$ is the nth zero point of the Bessel function $J_l(x)$, R is the radius of the cylinder.

For simplicity, we assume that the external magnetic field is applied along the z direction or x direction, i.e. parallel or perpendicular to the wire or rod. We can choose the symmetric gauge when the magnetic field is applied along the z direction. The vector potential is written as

$$\mathbf{A} = \left(-\frac{1}{2}B_z y, \frac{1}{2}B_z x, 0\right). \tag{9}$$

Table 1. The parameters used in this paper.

	m_c	L	M	N	E_P(eV)	E_g (eV)	Δ_{so} (eV)	ϵ_r
InAs	0.02226	54.2	3.87	55.6	21.6	0.418	0.38	15.15
InSb	0.0136	98.9	4.58	101.0	21.2	0.2352	0.81	16.8

When the magnetic field is applied along the x direction, for simplicity, we choose the Landau gauge, and vector potential is,

$$\mathbf{A} = (0, 0, B_x y). \tag{10}$$

In the presence of external magnetic field, the momentum operator changes into $\mathbf{p} \Rightarrow \mathbf{p}+e\mathbf{A}$. The whole Hamiltonian can be written as

$$H = H_{eb} + H^a_{asym} + H_{Zeeman} + H^a_{mm}, \tag{11}$$

where

$$H^a_{asym} = \begin{pmatrix} 0 & & \\ & H_{asym} & \\ & & 0 \\ & & & H_{asym} \end{pmatrix}, \tag{12}$$

and H_{asym} is given in details before [21]. H_{Zeeman} is the spin-Zeeman-splitting Hamiltonian, and H^a_{mm} is the remainder part, which is named as magnetic-momentum Hamiltonian. H^a_{mm} has the form

$$H^a_{mm} = \begin{pmatrix} H_{mm} & 0 \\ 0 & H_{mm} \end{pmatrix}, \tag{13}$$

where H_{mm} is a 4×4 matrix, which is given in Appendix A.

We also calculate the linear polarization factor of the short rods. We assume that the light wave propagates along the y direction. The linear polarization factor is given by

$$P = (I_z - I_x)/(I_z + I_x). \tag{14}$$

I_z and I_x are the intensities of z and x polarized transitions, which can be calculated similarly to the quantum ellipsoid case.

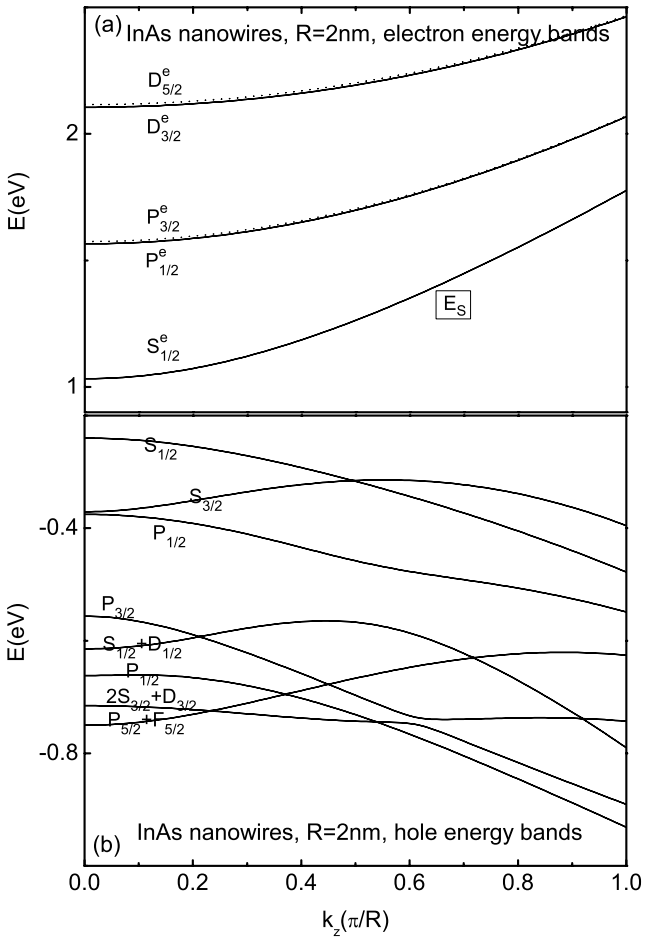

Fig. 1. Energy bands $E(k_z)$ of the InAs nanowires with radius of $R = 2$ nm. (a) Electron energy bands. (b) Hole energy bands.

3 Results and discussion

In this section, we calculate the electronic structure, optical properties and g factors of narrow-gap zinc-blende nanowires and nanorods. The parameters [22] used in this paper are listed in Table 1. However, these parameters measured in the bulk material include some contributions, say, nonlocal character of the self-consistent potential, that are absent in narrow-gap nanostructures [17]. Therefore, using these parameters requires taking special precautions. The nonlocal contributions are

$$\Delta L = -21\delta_{nl},\ \Delta M = 3\delta_{nl},\ \Delta N = -24\delta_{nl}, \tag{15}$$

$$\Delta\alpha = -10\delta_{nl},\ \delta_{nl} = \frac{2}{15\pi\epsilon_r E_g}\sqrt{\frac{E_B E_p}{3}}, \tag{16}$$

where $E_B = 27.211$ eV and ϵ_r is the dielectric constant given in Table 1.

3.1 Electronic structure

The energy bands $E(k_z)$ of the InAs nanowires with radius of $R = 2$ nm are shown in Figure 1. The symbol of each energy band represents the main components of it's wave function. For example, $S_{1/2}$ means that the state is a hole state and consists mainly of the $J = 1/2$, $l = 0$ and $n = 1$ state of the effective-mass envelope function [Eq. (7)] multiplied with the Bloch state and the spin state, and $S^e_{1/2}$ is a electron state. From Figure 1a we see that the electron energy bands are simple parabolic bands with the order S, P, and D. The P and D energy bands split due to the coupling of the conduction band and valence band. The energy of the $S^e_{1/2}$ energy band is denoted as E_s, which will be used later. Because J is a good quantum number, only the states with the same J are coupled. Due to the off-diagonal $p_\pm$-linear terms S^* and S in the Hamiltonian [Eq. (2)], the hole states with $\Delta l = \pm 1$ and $\Delta J = 0$ are

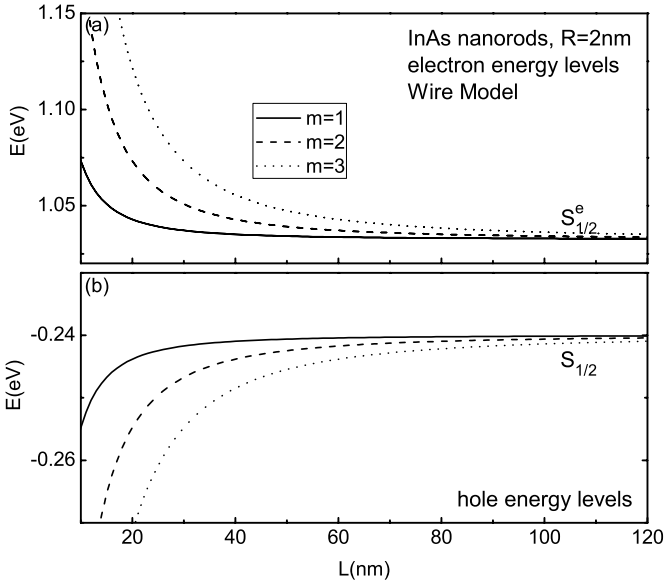

Fig. 2. Electron and hole energy levels of the InAs nanorods with $R = 2$ nm as functions of the length L calculated by the Wire Model. (a) Electron levels. (b) hole levels.

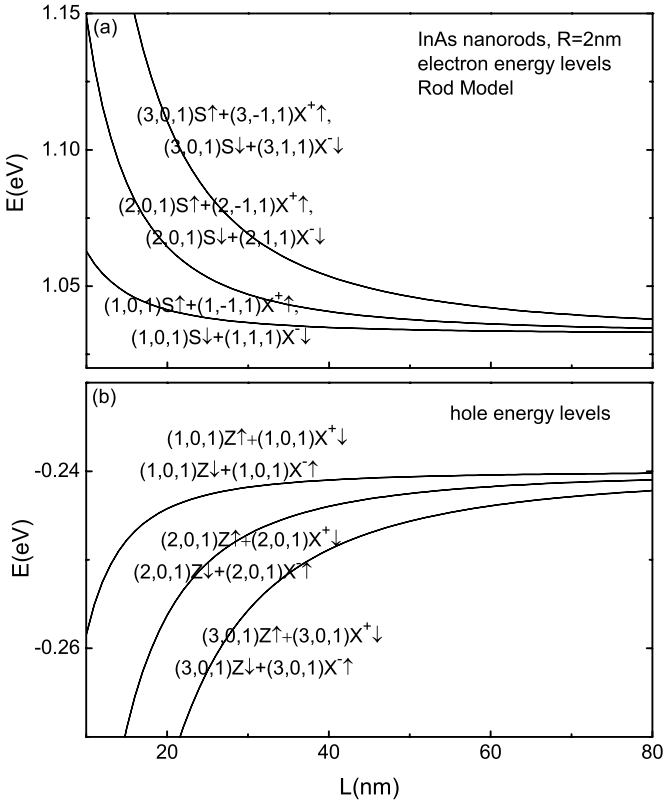

Fig. 3. Electron and hole energy levels of the InAs nanorods with $R = 2$ nm as functions of the length L calculated by the Rod Model. (a) Electron levels. (b) hole levels.

coupled, for example the state $P_{1/2}$ are coupled with the states $S_{1/2}$ and $S_{1/2} + D_{1/2}$, and the state $P_{3/2}$ are coupled with the states $S_{3/2}$ and $2S_{3/2} + D_{3/2}$, as shown in Figure 1b. The hole energy bands show a complex relation with k_z due to the coupling of the bands. The hole ground state is a S state.

The electron and hole energy levels of the InAs nanorods with $R = 2$ nm as functions of the length L are shown in Figures 2 and 3, calculated by the Wire Model and Rod Model respectively. The energy levels in Figures 2 and 3 are all two-fold degenerated. The Wire Model results are simply read from the corresponding energy bands in Figure 1 at the wave vector $k_z = m\pi/L$, $m = 1, 2, 3$. The symbol of each energy level in Figure 3 represents the main components of it's wave function. For example, $(2, 0, 1)S\uparrow$ means that the state consists mainly of the $m = 2$, $l = 0$, $n = 1$ state of the effective-mass envelope function [Eq. (7)] multiplied with the S Bloch state of the conduction-band bottom and the spin-up state. We see that the energy levels decrease with the length increasing. The electron states [see Fig. 3a] consist of many hole-state components, due to the coupling of the conduction band and valence band. We see that the level symbols in Figures 3a and 3b are similar respectively, only the m-numbers change. Actually, the rest part of the symbols represent the main components of the states of the corresponding energy bands in Figure 1, and the m-numbers are similar to those in Figure 2. Moreover the energy levels in Figure 2 are in agreement with those in Figure 3. So the Wire Model is in agreement with the Rod Model, i.e. these energy levels can be modelled by the Wire Model.

The energy bands $E(k_z)$ of the InSb nanowires are shown in Figures 4 and 5. We see that Figure 4b is similar to Figure 1b, both the highest hole states are at $k_z = 0$ point. Actually, all the electron bands and hole

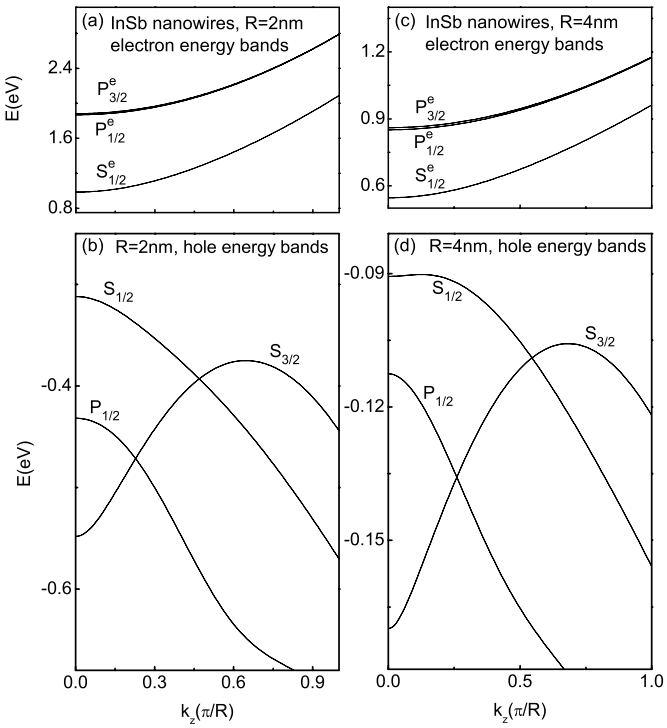

Fig. 4. Energy bands $E(k_z)$ of the InSb nanowires. (a) $R = 2$ nm, electron bands. (b) $R = 2$ nm, hole bands. (c) $R = 4$ nm, electron bands. (d) $R = 4$ nm, hole bands.

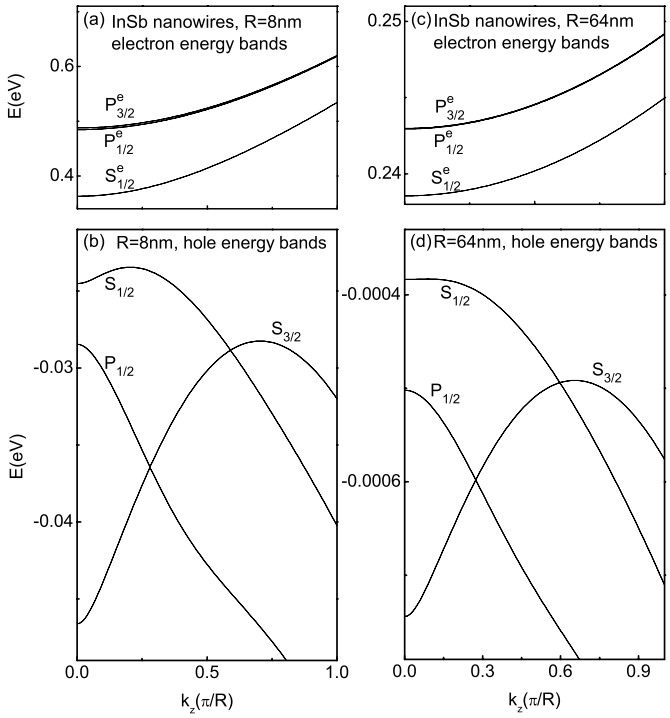

Fig. 5. Energy bands $E(k_z)$ of the InSb nanowires. (a) $R = 8$ nm, electron bands. (b) $R = 8$ nm, hole bands. (c) $R = 64$ nm, electron bands. (d) $R = 64$ nm, hole bands.

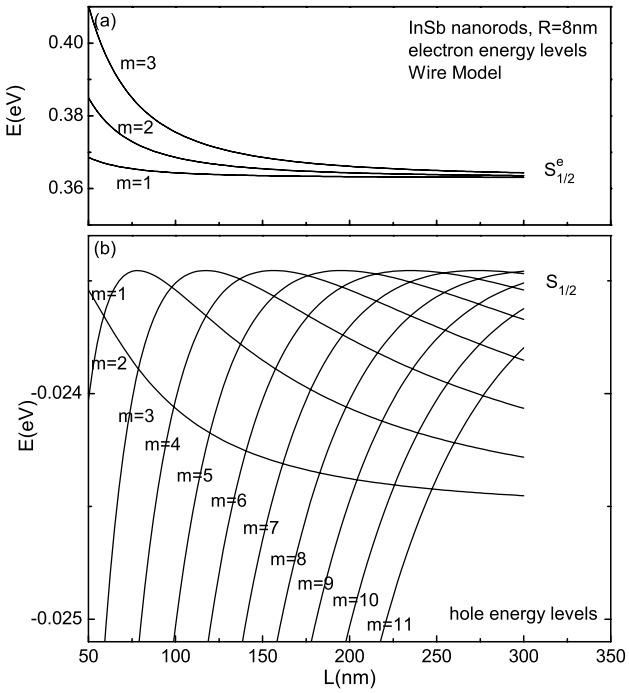

Fig. 6. Electron and hole energy levels of the InSb nanorods with radius of $R = 8$ nm as functions of the length L calculated by the Wire Model. (a) Electron levels. (b) Hole levels.

bands in Figures 1, 4 and 5 are similar respectively, little change happens. But this change is important. It is noticed that the highest hole states in Figures 4d, 5b and 5d are not at $k_z = 0$ point, while at $k_z = 0.1021$ nm^{-1}, $k_z = 0.0785$ nm^{-1} and $k_z = 0.0044$ nm^{-1} points, respectively. That means that they have indirect band gaps. The the $R = 8$ nm case in Figure 5b is the most obviously, the $P_{1/2}$ band couple with the $S_{1/2}$ band strongly leading to the hump of the latter band. Actually, the coupling of the $P_{1/2}$ band and $S_{1/2}$ band is mainly introduced by the off-diagonal $p_{\pm}$-linear terms S^* and S in the Hamiltonian [Eq. (2)]. Because the S^* and S terms are also p_z-linear terms, the states are coupled more strongly when the k_z ($=p_z/\hbar$) is larger. This causes the $S_{1/2}$ energy band increases with the k_z increasing when k_z is small. When k_z is large, the $S_{1/2}$ energy band decreases with the k_z increasing, due to the p_z-quadratic terms [see Eq. (2)]. The $S_{3/2}$ bands in Figures 4 and 5 and the $S_{3/2}$, $S_{1/2} + D_{1/2}$, $P_{5/2} + F_{5/2}$ energy bands in Figure 1 vary in the similar way, due to the similar reason to the $S_{1/2}$ energy band in Figures 4d and 5, and their highest points are also not the $k_z = 0$ point. But indirect band gap only happens in certain condition. The indirect band gap is mainly due to the coupling of the $S_{1/2}$ and $P_{1/2}$ bands. When the radius is very small, the $S_{1/2}$ and $P_{1/2}$ bands are too far away, the coupling is so small that it can not bring an indirect band gap, as shown in Figure 4b. When the radius is too large, the $S_{1/2}$ and $P_{1/2}$ bands are close, but the coupling $p_{\pm}$-linear (i.e. $\frac{1}{R}$-linear) terms S^* and S are so small that they can not bring an indirect band gap. For InSb case, when the radius is approximately in the range of $[4, 64]$ nm, the coupling of the $S_{1/2}$ and $P_{1/2}$ bands is strong enough to bring the indirect band gaps. When R is as large as that the nanowires can be treated as bulk materials, the band gap should be direct. For InAs case, the coupling is always not strong enough. The variation of the coupling strength can also be seen from the electron bands in Figures 4a, 4c, 5a and 5c. The splitting of the electron P bands are due to their coupling with the hole S and D bands. When the radius is very small, the coupling bands are too far away. When the radius is very large, the coupling is too small. When R is as large as that the nanowires can be treated as bulk materials, there should be no splitting. So only in the moderate radius case, the splitting can be seen explicitly, as shown in Figures 4c and 5a.

The electron and hole energy levels of the InSb nanorods with $R = 8$ nm as functions of the length L are shown in Figures 6 and 7, calculated by the Wire Model and Rod Model respectively. The energy levels in Figures 6 and 7 are all two-fold degenerated. The Wire Model results are simply read from the corresponding energy bands in Figures 5a and 5b at the wave vector $k_z = m\pi/L$, respectively. We see that the energy levels in Figure 6a are in agreement with those in Figure 7a, i.e. these energy levels can be modelled by the Wire Model. So we label the levels in Figure 7a as $S^e_{1/2}m$, $m = 1, 2, 3$. We only show the lowest three levels because this case is very simple. While the hole case is complicated as shown in Figures 6b and 7b.

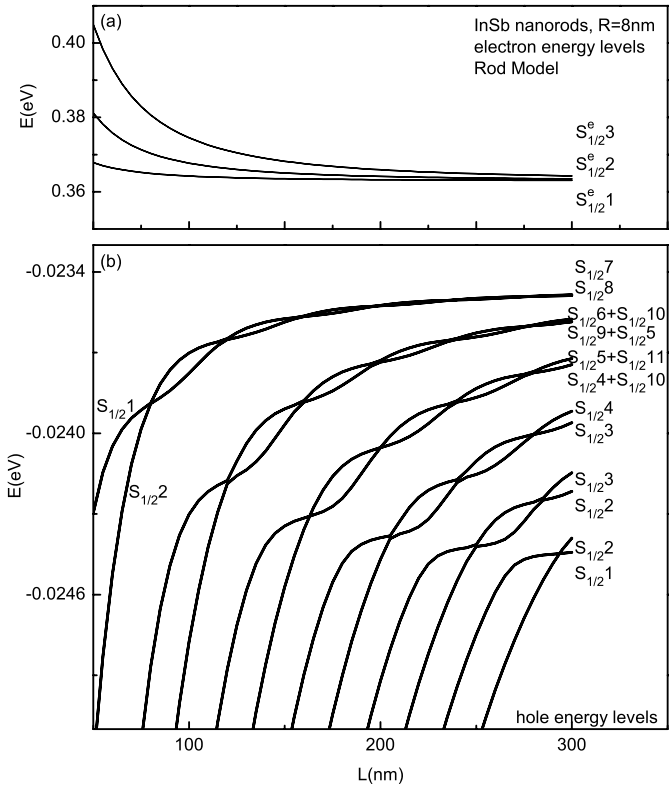

Fig. 7. Electron and hole energy levels of the InSb nanorods with radius of $R = 8$ nm as functions of the length L calculated by the Rod Model. (a) Electron levels. (b) Hole levels.

First of all, Figure 6b is not in agreement with Figure 7b, i.e. these levels can not be modelled by the Wire Model (but we label the levels by the similar symbols in Figure 7a approximately). The reason is that there are many crossing points of different m levels in Figure 6b. These levels do not couple with each other because the Wire Model ignores their couplings. In Rod Model, the m levels with different parities couple with each other, leading to the interesting plait-like pattern. However, the Wire Model results in Figure 6b also give some hints of the real case. For example, for a given L, the highest hole level is the level (labelled by m) whose corresponding wave vector is at the lowest point in Figure 5b, saying

$$m\frac{\pi}{L} = 0.0785. \tag{17}$$

As we see, when $L = 50$ nm, $m \approx 1$, the highest level in Figure 6b is the $m = 1$ level, which hints the highest states in Figure 7b are mainly $m = 1$ states. When $L = 300$ nm, $m \approx 7$, the highest level in Figure 6b is the $m = 7$ level, which in agreement with that the highest states in Figure 7b are mainly $m = 7$ states. In Figure 6b the $m = 1$ level decreases with increasing L, and in Figure 7b the $m = 1$ states move down as L increases, which also happens for other m states.

Actually the other bands in Figures 1, 4 and 5, which are not monotone functions of $|k_z|$, for example, the $S_{3/2}$ bands in Figures 4 and 5 and the $S_{3/2}$, $S_{1/2} + D_{1/2}$, $P_{5/2} + F_{5/2}$ bands in Figure 1, can not be modelled by the Wire Model due to the similar reason. Only the normal bands which are monotone functions of $|k_z|$, for example, electron bands and $S_{1/2}$ bands in Figures 1b and 4b, can be modelled by the Wire Model.

3.2 Linear polarization of InAs rods

The linear polarization factor of the InAs nanorods with radius of $R = 2$ nm at temperature of $T = 300$ K as a function of the length L is shown in Figure 8a. We see that as the L increases, the linear polarization factor changes from -1 to 0.8. When $L = 3.54$ nm, and the corresponding aspect ratio $L/2R = 0.885 < 1$, the polarization factor is zero. The normalized intensities of the InAs nanorods with $R = 2$ nm at $T = 300$ K as functions of the L are shown in Figure 8b. We see that as the L increases, the normalized intensity I_x decreases, and the normalized intensity I_z increases at first, resulting in the increase of the polarization factor, then they both decrease slowly due to the decrease of the overlap of the electron and hole wave functions when L is sufficiently large. The linear polarization factor of the InSb nanorods with radius of $R = 2$ nm at temperature of $T = 300$ K as a function of the length L is shown in Figure 8c. We see that the polarization factor is a little smaller than the InAs case, and is zero when $L/2R = 0.8475$.

3.3 Magnetic energy levels and g factors

The hole magnetic energy levels and the g_z factors of the InAs nanowires with $R = 2$ nm in the magnetic field $B = 20$ Tesla as functions of the k_z are shown in Figures 9a and 9b, respectively. The g factor is defined as,

$$\Delta E = g\mu_B B, \tag{18}$$

where ΔE is the splitting energy. From Figure 9b we see that the g_z factor of the hole state $S_{1/2}$ decreases from 1 at $k_z = 0$ to 0 at $k_z \approx 0.5\ \pi/R$, then increases when the k_z increases continuously. The electron magnetic energy levels and the g_z factors of the nanowires with $R = 2$ nm as functions of the k_z are shown in Figures 9c and 9d, respectively. From Figure 9d we see that the g_z factor of the electron ground state increases from 0.93 at $k_z = 0$ as the k_z increases. From the variation of the g_z factor of the nanowires with the k_z we can obtain the g_z factor of the nanorods as functions of the L.

By expanding the longitudinal function with the Sine functions [Eq. (5)] we calculate the magnetic energy levels in the external magnetic field applied along the z and x directions, i.e. parallel and perpendicular to the rod. The g factors of the electron ground state of the InAs nanorods with $L = 2$ nm as functions of the R are shown in Figure 10a. We see that the g factors decrease as the radius increases. The g_z factor decreases more than the g_x factor. Actually, as the radius increases, two dimensions

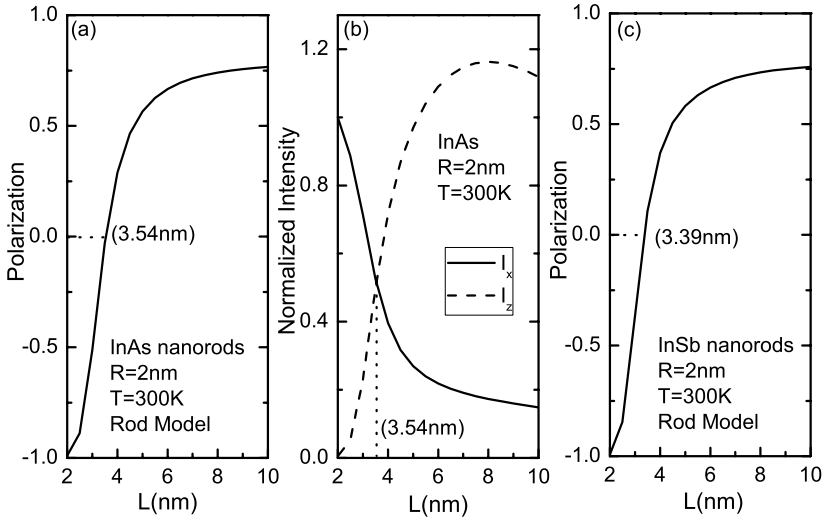

Fig. 8. (a) The linear polarization factor of the InAs nanorods with radius of $R = 2$ nm at temperature of $T = 300$ K as a function of the length L calculated by the Rod Model. (b) Normalized intensities of the InAs nanorods with $R = 2$ nm at $T = 300$ K as functions of the L. (c) The linear polarization factor of the InSb nanorods with radius of $R = 2$ nm at temperature of $T = 300$ K as a function of the length L calculated by the Rod Model.

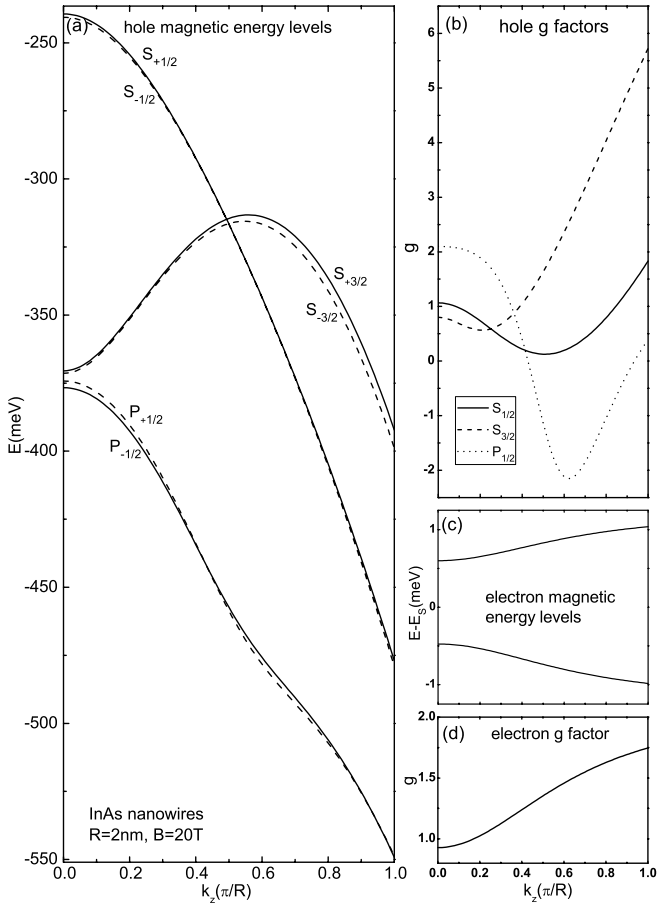

Fig. 9. (a) The hole magnetic energy levels and (b) the g_z factors, and (c) the electron magnetic energy levels and (d) the g_z factors of the InAs nanowires with $R = 2$ nm in the magnetic field $B = 20$ Tesla as functions of the k_z. The electron magnetic energy levels subtract the energy E_s which is shown in Figure 1a.

perpendicular to the z direction relax, one dimension perpendicular to the x direction relaxes. We assume that the dimensions perpendicular to the direction of the magnetic field affect the g factors more than the other dimension. In this case, the increasing radius affects the g_z factor more than g_x.

The g factors of the electron ground state of the InAs nanorods with $R = 2$ nm as functions of the L calculated by the Rod Model are shown in Figure 10b. From Figure 10b we see that the g factors decrease as the length L increases, and the g_x factor decreases more than the g_z factor. In this case the increasing length increases space in the z direction, so affects the g_x factor more than g_z. The g_z factor decreases from 1.0 for $L = 10$ nm to 0.93 for $L = 80$ nm, which is in agreement with the g_z factor of the nanowires with $R = 2$ nm [Fig. 9d] for the k_z changing from $0.2\pi/R$ to $0.025\pi/R$, i.e. the Rod Model accords with the Wire Model in this case.

The g factors of the hole ground state of the InAs nanorods with $R = 2$ nm as functions of the L calculated by the Rod Model are shown in Figure 10c. We see that the g_x factor decreases as the length increases, which is similar to the electron g factors (see Figs. 10a and 10b). It is noticed that the g_z factor increases from 0.8 for $L = 10$ nm to 1.05 for $L = 80$ nm, which is in agreement with the g_z factor of the hole state $S_{1/2}$ of the nanowires with $R = 2$ nm [Fig. 9b] for the k_z changing from $0.2\pi/R$ to $0.025\pi/R$, i.e. the Wire Model works for this $S_{1/2}$ band (see Fig. 1b).

The g factors of InSb nanowires (nanorods) with radius of $R = 2$ nm as functions of the k_z (L) are shown in Figure 11. The rod case is calculated in the Rod Model. We see that the g factors are very similar to the InAs case. As the lowest hole band in Figure 4b is similar to that in Figure 1b for which the Wire Model works, we can also do the comparison between the g factors of nanowires and nanorods, similarly to Figures 9 and 10.

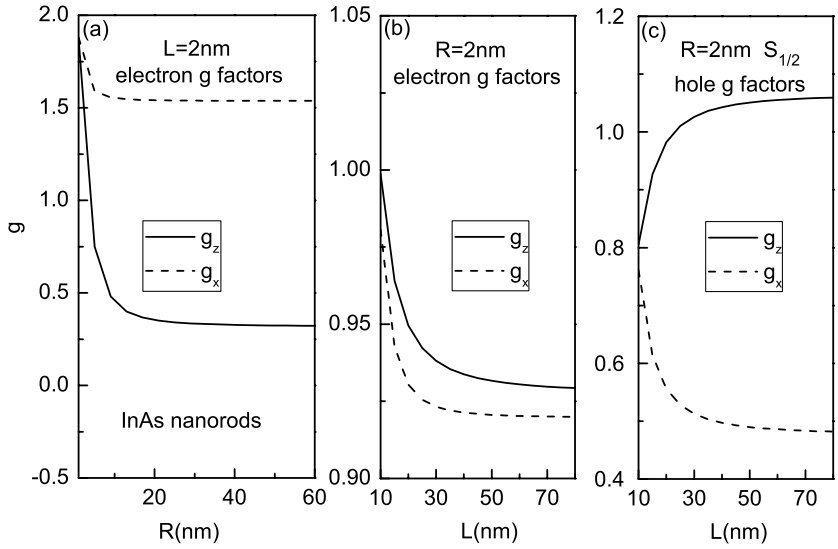

Fig. 10. The g factors of the electron/hole ground state of the InAs nanorods calculated by the Rod Model. (a) $L = 2$ nm, electron g factors as functions of the R. (b) $R = 2$ nm, electron g factors as functions of the L. (c) $R = 2$ nm, hole g factors as functions of the L.

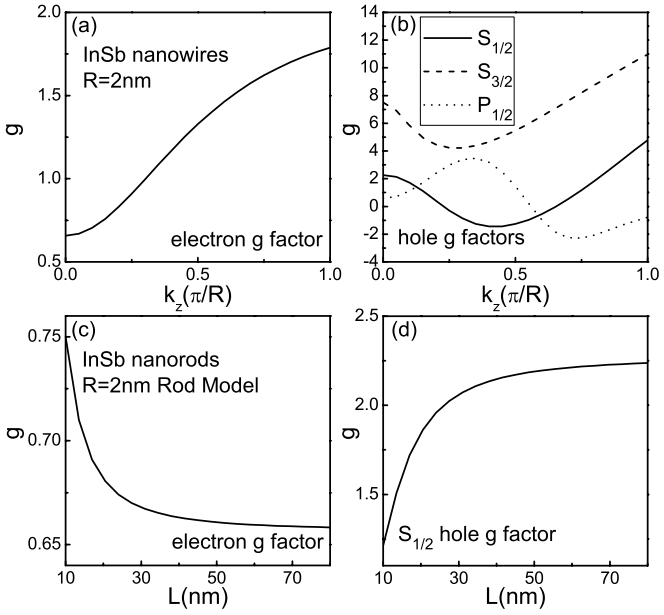

Fig. 11. The g factors of InSb nanowires (nanorods) with radius of $R = 2$ nm as functions of the k_z (L). The rod case is calculated in the Rod Model. (a) Nanowires, electron g factor. (b) Nanowires, hole g factors. (c) Nanorods, electron g factor. (d) Nanorods, hole g factor.

4 Conclusions

The Hamiltonian in the framework of eight-band effective-mass approximation of the zinc-blende nanowires and nanorods in the presence of external homogeneous magnetic field is given in the cylindrical coordinate. The electronic structure, optical properties, magnetic energy levels, and g factors of nanowires and nanorods are calculated. The electron states consist of many hole-state components, due to the coupling of conduction band and valence band. For the normal bands the Wire Model works, the energy levels of the nanorods approximately equal the values of the energy band $E(k_z)$ of the nanowires with the same radius at a special k_z. Because the hole states with $\Delta l = \pm 1$ and $\Delta J = 0$ are coupled by the S^* and S terms in the Hamiltonian [Eq. (2)], some of the hole energy bands of the nanowires have their highest points at $k_z \neq 0$. Especially, the highest hole state of the InSb nanowires is not at the $k_z = 0$ point. It is an indirect band gap. And the indirect band gap is the most obvious when the wire is moderately thicker. For these abnormal bands, the Wire Model is wrong. The energy levels of the nanorods show an interesting plait-like pattern. The linear polarization factor is zero, when the aspect ratio $L/2R$ is smaller than 1, and increases as the length increases. The g_z and g_x factors as functions of the k_z, radius R and length L are calculated for wires and rods, respectively. For the wires, the g_z factor of the electron ground state increases, and the g_z of the hole ground state decreases first, then increases with the k_z increasing. For the rods, the g_z and g_x factors of the electron ground state decrease as the R or the L increases. The g_x of the hole ground state decreases, the g_z of the hole ground state increases with the L increasing. The variation of the g_z factor of wires with the k_z is in agreement with the variation of the g_z of rods with the L.

This work was supported by the National Natural Science Foundation No. 90301007, 60521001 and the special funds for Major State Basic Research Project No. G001CB3095 of China.

$$H_{mm} = \frac{1}{2m_0}$$

$$\begin{pmatrix}
\alpha(\frac{i}{2}eB(r_+p_- - r_-p_+) + \frac{1}{4}e^2B^2r_-r_+) & -\frac{1}{2\sqrt{2}}p_0eBr_+ & 0 & \frac{1}{2\sqrt{2}}p_0eBr_- \\
-\frac{1}{2\sqrt{2}}p_0eBr_- & -\frac{L'+M'}{2}(\frac{i}{2}eB(r_+p_- - r_-p_+) + \frac{1}{4}e^2B^2r_-r_+) & \frac{i}{2\sqrt{2}}N'eBr_-p_z & -\frac{L'-M'-N'}{4}(ieBr_+p_+ - \frac{1}{4}e^2B^2r_+^2) + \frac{L'-M'+N'}{4}(ieBr_-p_- + \frac{1}{4}e^2B^2r_-^2) \\
0 & -\frac{i}{2\sqrt{2}}N'eBr_+p_z & -M'(\frac{i}{2}eB(r_+p_- - r_-p_+) + \frac{1}{4}e^2B^2r_-r_+) & \frac{i}{2\sqrt{2}}N'eBr_-p_z \\
\frac{1}{2\sqrt{2}}p_0eBr_+ & \frac{L'-M'-N'}{4}(ieBr_-p_- + \frac{1}{4}e^2B^2r_-^2) - \frac{L'-M'+N'}{4}(ieBr_+p_+ - \frac{1}{4}e^2B^2r_+^2) & -\frac{i}{2\sqrt{2}}N'eBr_+p_z & -\frac{L'+M'}{2}(\frac{i}{2}eB(r_+p_- - r_-p_+) + \frac{1}{4}e^2B^2r_-r_+)
\end{pmatrix}. \tag{A.19}$$

$$H_{mm} = \frac{1}{2m_0}$$

$$\begin{pmatrix}
\alpha(ieBr_-p_z - ieBr_+p_z - \frac{1}{4}e^2B^2r_+^2 - \frac{1}{4}e^2B^2r_-^2 + \frac{1}{2}e^2B^2r_-r_+) & 0 & \frac{1}{2}p_0eB(r_+ - r_-) & 0 \\
0 & -M'(ieBr_-p_z - ieBr_+p_z - \frac{1}{4}e^2B^2r_+^2 - \frac{1}{4}e^2B^2r_-^2 + \frac{1}{2}e^2B^2r_-r_+) & -\frac{i}{2\sqrt{2}}N'(eBr_-p_- - eBr_+p_- + ieB\hbar) & 0 \\
-\frac{1}{2}p_0eB(r_+ - r_-) & -\frac{i}{2\sqrt{2}}N'(eBr_-p_+ - eBr_+p_+ - ieB\hbar) & -L'(ieBr_-p_z - ieBr_+p_z - \frac{1}{4}e^2B^2r_+^2 - \frac{1}{4}e^2B^2r_-^2 + \frac{1}{2}e^2B^2r_-r_+) & -\frac{i}{2\sqrt{2}}N'(eBr_-p_- - eBr_+p_- + ieB\hbar) \\
0 & 0 & -\frac{i}{2\sqrt{2}}N'(eBr_-p_+ - eBr_+p_+ - ieB\hbar) & -M'(ieBr_-p_z - ieBr_+p_z - \frac{1}{4}e^2B^2r_+^2 - \frac{1}{4}e^2B^2r_-^2 + \frac{1}{2}e^2B^2r_-r_+)
\end{pmatrix}. \tag{A.20}$$

Appendix A

In this appendix, we give the form of H_{mm} in equation (13). When the magnetic field is applied along the z direction ($B = B_z$), H_{mm} is written as

see equation (A.19) above

When the magnetic field is applied along the x direction ($B = B_x$), H_{mm} is written as

see equation (A.20) above.

References

1. M. He, M.M.E. Fahmi, S.N. Mohammad, R.N. Jacobs, L. Salamanca-Riba, F. Felt, M. Jah, A. Sharma, D. Lakins, Appl. Phys. Lett. **82**, 3749 (2003)
2. S. Kan, T. Mokari, E. Rothenberg, U. Banin, Nature **2**, 155 (2003)
3. D. Steiner, D. Katz, O. Millo, A. Aharoni, S. Kan, T. Mokari, U. Banin, Nano Lett. **4**, 1073 (2004)
4. S. Banerjee, A. Dan, D. Chakravorty, J. Mater. Sci. **37**, 4261 (2002)

5. M. Law, J. Goldberger, P. Yang, Annu. Rev. Mater. Res. **34**, 83 (2004)
6. S.V. Zaitsev-Zotov, Yu A. Kumzerov, Yu A. Firsov, P. Monceau, J. Phys.: Condens. Matter **12**, L303 (2000)
7. P.C. Sercel, K.J. Vahala, Phys. Rev. B **42**, 3690 (1990)
8. S. Çakmak, Zeitschrift für Naturforschung A **60**, 593 (2005)
9. C.E. Pryor, M.E. Flatt, Phys. Rev. Lett. **96**, 026804 (2006)
10. S. Çakmak, A.M. Babayev, E. Artunç, A. Kőkçe, S. Çakmaktepe, Physica E **18**, 365 (2003)
11. J. Wang, M.S. Gudiksen, X. Duan, Yi Cui, C.M. Lieber, Science **293**, 1455 (2001)
12. C.L. Romano, S.E. Ulloa, P.I. Tamborenea, Phys. Rev. B **71**, 035336 (2005)
13. A. Shabaev, Al. L. Efros, Nano Lett. **4**, 1821 (2004)
14. S. Baskoutas, Chem. Phys. Lett. **404**, 107 (2005)
15. T. Someya, H. Akiyama, H. Sakaki, Phys. Rev. Lett. **76**, 2965 (1996)
16. J.C. Johnson, H.-J. Choi, K.P. Knutsen, R.D. Schaller, P. Yang, R.J. Saykally, Nature **1**, 106 (2002)
17. Al. L. Efros, M. Rosen, Phys. Rev. B **58**, 7120 (1998)
18. E.O. Kane, *Handbook on Semiconductors*, edited by W. Paul, T.S. Moss (North-Holland, 1982), Vol. 1
19. M.H. Weiler, J. Magn. Magn. Mater. **11**, 131 (1979)
20. D. Katz, T. Wizansky, O. Millo, E. Rothenberg, T. Mokari, U. Banin, Phys. Rev. Lett. **89**, 086801 (2002)
21. J.M. Luttinger, Phys. Rev. B **102**, 1030 (1956)
22. Landolt-Börnstein, Group III, **17** a.